



Monte Carlo modeling of recrystallization processes in α -uranium

M.A. Steiner ^{a,*}, R.J. McCabe ^b, E. Garlea ^c, S.R. Agnew ^a

^a University of Virginia, Material Science and Engineering, 395 McCormick Rd, Charlottesville, VA 22904, USA

^b Materials Science and Technology Division, Los Alamos National Laboratory, Los Alamos, NM, USA

^c Y-12 National Security Complex, Oak Ridge, TN 37831, USA

HIGHLIGHTS

- Monte Carlo modelling and experimental EBSD data are used to simulate static recrystallization textures in α -uranium.
- Consistent with prior observations, recrystallized nuclei form on non-twin high-angle grain boundary sites at 450 °C.
- In a new finding, nucleation occurs only at a highly constrained subset of boundary sites with the most local deformation.
- The results can be incorporated into ab initio microstructural simulations to predict final recrystallized microstructures.

ARTICLE INFO

Article history:

Received 26 October 2016

Received in revised form

23 March 2017

Accepted 20 April 2017

Available online 22 April 2017

Keywords:

α -Uranium

Recrystallization

Monte carlo

Potts modeling

EBSD

ABSTRACT

Starting with electron backscattered diffraction (EBSD) data obtained from a warm clock-rolled α -uranium deformation microstructure, a Potts Monte Carlo model was used to simulate static site-saturated recrystallization and test which recrystallization nucleation conditions within the microstructure are best validated by experimental observations. The simulations support prior observations that recrystallized nuclei within α -uranium form preferentially on non-twin high-angle grain boundary sites at 450 °C. They also demonstrate, in a new finding, that nucleation along these boundaries occurs only at a highly constrained subset of sites possessing the largest degrees of local deformation. Deformation in the EBSD data can be identified by the Kernel Average Misorientation (KAM), which may be considered as a proxy for the local geometrically necessary dislocation (GND) density.

© 2017 Elsevier B.V. All rights reserved.

1. Introduction

Uranium components are typically produced in a similar manner to many other metals, starting from cast material that undergoes a series of thermomechanical processes such as forging, rolling, swaging and forming. Deformation processing steps are frequently interspersed with heat treatments to produce finer, recrystallized grains and restore ductility. Along with having significant effects on grain size and morphology, thermomechanical processes can cause significant evolution in a material's crystallographic texture. The crystallographic texture of uranium is often of critical interest because the low temperature allotrope, the orthorhombic α -phase, has unique anisotropic properties including a negative thermal expansion coefficient along one crystallographic direction [1–4]. A number of investigations in the last decade have

explored the microstructural and textural evolution of α -uranium during different types of deformation [5–12]. While post-deformation recrystallization phenomena and associated modeling approaches are well documented for a number of predominantly cubic metals [13–17], comparatively less study has been made into the recrystallization processes governing metals of lower symmetry. Lower symmetry crystal structures generally deform via several distinct modes of dislocation slip and deformation twinning, the relative activities of which are sensitive to grain orientation and temperature. These slip and twinning modes are known to control the evolution of deformation textures, and in turn could impact the textures evolution during recovery and recrystallization. This is especially true for α -uranium, which has four distinct dislocation slip modes and at least three modes of deformation twinning, many with multiple slip systems or variants [6,18,19]. While it is likely that recrystallization in α -uranium proceeds through a process comparable to that of higher symmetry metals, efforts to establish the exact nature of this process have

* Corresponding author.

E-mail address: mas4cw@virginia.edu (M.A. Steiner).

been hampered by the limited amount of experimental data available in the literature. A number of empirical studies on the recrystallization of α -uranium were carried out into the early 1960s, but the crystallographic texture analysis was rudimentary [20–27] and the data generated in these studies cannot be correlated to individual grains in a manner necessary for developing mechanistic models or improving upon the existing phenomenological understanding. It was established, however, that the crystallographic texture of annealed α -uranium is site-saturated (all nuclei form near the onset of recrystallization), and dependent on both the deformation geometry and the recrystallization temperature [20].

Static recrystallization occurs by the migration of high-angle grain boundaries (HAGBs) driven by the release of stored deformation energy, leading to a new microstructure of relatively defect-free grains. It has been established that the nuclei of recrystallized grains already exist in deformed microstructures (or coalesce prior to recrystallization during static or dynamic recovery) [13–17]. These nuclei do not always originate from the dominant crystallographic orientations of the deformed microstructure, and thus, their growth can lead to texture evolution. Both the formation of these recrystallized nuclei and the stored energy that induces their expansion through the deformed microstructure are heavily impacted by the type and degree of deformation, as well as grain orientation, size, shape, and distribution. To establish an understanding of recrystallization in α -uranium on a level comparable to cubic metals, detailed microstructural analysis of deformed and subsequently recrystallized samples is necessary.

Electron backscattered diffraction (EBSD) is an ideal tool for characterizing recrystallization as it provides statistically significant, spatially sensitive crystallographic information at the sub-granular scale. This allows for construction not only of the sample's collective crystallographic texture, but also structural features at specific locations, including grain orientation, grain boundary geometry, and intra-granular misorientation due to deformation. Successful preparation of α -uranium samples for EBSD analysis is notoriously difficult [28–30]. In addition to radiological safety concerns, the surface of uranium metal rapidly oxidizes upon exposure to air. The challenges of oxidation are exacerbated by the high atomic number of uranium, which restricts the interaction volume of backscattered electrons and prevents interrogation of the metal beneath all but the thinnest of oxide layers. Despite these difficulties, high quality EBSD data of warm-rolled α -uranium before, during, and after recrystallization at 450 °C has recently been published by one of the authors [31]. Comparing the texture of the recrystallized microstructure to that of select components within the deformed microstructure, it was noted that the varying degrees of deformation present in grains of different orientations does not explain the observed crystallographic texture evolution during recrystallization [31]. Instead, the collective texture of points found along non-twin HAGBs is a closer match to the recrystallized texture, suggesting that recrystallized nuclei at 450 °C form primarily along these boundaries.

It is possible to simulate recrystallization within a microstructure that has been characterized by EBSD through a number of different techniques, including cellular automata, phase field, and Monte Carlo models [32–34]. One of the biggest challenges for all of these models is determining the nucleation parameters governing the formation and location of recrystallized nuclei [34], which are hard to determine *a priori* and must be informed by comparing experimental and simulated results. The simulations in the present study were performed utilizing a Monte Carlo (MC) technique known as Potts modeling. MC Potts modeling is a generalization of the simpler Ising model to systems with more

than two states (e.g. unique grain orientations) [35–37], and has long been used to simulate grain growth phenomena within recrystallized microstructures [35,36]. Subsequent expansions of the model have been successfully employed to simulate recrystallization as well as grain growth, starting from deformed microstructures [38–41].

The Potts model begins with a 2D or 3D lattice, where each point is assigned to a specific grain and the lattice is sized so that each grain contains a significant number of lattice points at initialization. Driven by a minimization of energy, the Potts model uses probabilistic methods to test small changes on the local scale, preferentially keeping changes that decrease the system's energy. When modeling recrystallization through the Potts framework, the total energy of the system can be expressed by the following Hamiltonian:

$$H = \sum_{i=1}^N \left\{ E_i + \frac{1}{2} \sum_{j=1}^Z \gamma_{ij} \right\} \quad (1)$$

where E_i is the stored energy at site i (above a recrystallized ground state), γ_{ij} is the grain boundary energy between sites i and j summed over Z nearest neighbors (halved to prevent double counting), and both energy contributions are summed over all N -sites [40].

A simulation microstructure in the Potts model can be populated directly from experimental EBSD data, allowing each lattice site to be assigned a unique set of Euler angles according to the measured orientation. For a 2D square lattice, such as that used in this study, each lattice point can be considered to share eight neighbors (including diagonals). When two neighboring lattice sites in the simulation are assigned to different grains, their interface represents a grain boundary segment with an associated grain boundary energy. For most materials, the boundary energy can be defined as a function of the grain misorientation, based on the Read-Shockley model [42,43] together with the energies of special boundaries corresponding to the coincident site lattice model and additional elements as necessary.

If the simulation is being initialized by an *ab initio* computational technique that provides a fully quantified simulated microstructure (e.g. an N -site VPSC model [39], finite element model [41], or fast Fourier transform based [44] full-field crystal plasticity model) determining the stored energy from deformation, E_i , is straightforward. The assignment of stored energy to lattice sites based on experimental data is more complicated and requires extraction of quantities related to deformation from the EBSD map. The Image Quality (IQ) factor is a value that measures the sharpness of bands in the backscattered electron Kikuchi pattern used to index EBSD patterns. IQ is affected by gradients in the amount of local elastic strain present at each lattice point, allowing it to detect the difference between recrystallized and non-recrystallized grains [45–48], and it is possible to derive an empirical relationship between IQ and the stored elastic energy of a material [40]. Stored energy can also be related to the Kernel Average Misorientation (KAM) of each lattice point in the structure [49–57]. KAM is defined for a given lattice point as the average misorientation from other points of the same grain located inside a surrounding kernel of specified size, e.g. a second nearest-neighbor 5×5 grid, and correlates directly with the underlying geometrically necessary dislocation (GND) density. While the GND density represents only the minimum stored energy (held within the elastic strain fields of the dislocations) at a lattice location, it is a reasonable approximation that additional dislocations will share a similar distribution,

so that the total stored dislocation energy and KAM will exhibit an approximately linear relationship. When utilizing either IQ or KAM, the measured values must be placed in units of energy that are properly scaled to the grain boundary energy γ , and both techniques have inherent problems; IQ will vary with factors such as the surface quality of the prepared sample, EBSD parameters, and EBSD pattern filtering, while KAM only permits an indirect (though often accurate [56,57]) approximation of the total stored dislocation density. In the case of α -uranium, which has propensity to rapidly oxidize and requires EBSD pattern filtering, KAM becomes the logical proxy for stored energy as it is less dependent than IQ on the surface state of the material [30].

Once a microstructure and its governing energetics have been established, the Potts model executes, in series, a string of independent “events” at discrete lattice points within the microstructure, following a randomized order with one event executed at each site per simulation time step. During each event, the simulation will randomly select a lattice site neighboring the event site and test the change of energy that would result from replacing the event site with the neighboring site’s assignment, preferentially keeping the replacement and growing the neighboring grain when it decreases the energy of the system ($\Delta H < 0$). Through this stochastic process, the model is able to simulate evolution of the experimental microstructure and the resulting crystallographic texture. There are, however, several deficiencies to the standard formulation of the MC Potts model, including curvature artifacts related to the lattice, scaling of simulation units to physical units, and the concepts of real time and temperature not being explicitly tracked or handled. Improved formulations of the MC Potts model have been introduced to handle each of these issues and promote its predictive power [58–61].

This paper uses a very simple implementation of the Potts MC model as adapted to recrystallization, along with EBSD data from warm-rolled α -uranium originally published in Ref. [31] (Fig. 1), to simulate textures resulting from different assignments of recrystallized nuclei within the deformed microstructure. By comparing the textures simulated from different nuclei assignments to experimental recrystallization textures, the most likely locations of recrystallized nuclei in the warm clock-rolled α -uranium microstructure are determined. These nuclei conditions can be used to inform how recrystallization progresses in α -uranium deformation microstructures simulated using *ab initio* crystal plasticity based computational techniques.

2. Experimental methods

The experimental EBSD maps presented within this paper were acquired during the study in Ref. [31]. The α -uranium samples were warm clock-rolled at 300 °C in eight equivalent strain passes, with rotations of 0°, 90°, 135°, 225°, 270°, 360°, 45°, and 135°, resulting in a final reduction of approximately 50%. Clock-rolling is known to produce less in-plane texture anisotropy than unidirectional rolling of uranium [62] [63]. The warm-rolling temperature was considerably below the threshold that static recrystallization is observed to occur within uranium samples rolled to similar levels of deformation; with recrystallization taking approximately 100 h to complete at 380 °C and becoming kinetically limited below 350 °C [20]. In addition, dynamic recrystallization is not expected below 400 °C [64]. The recrystallized condition presented was heat treated under vacuum in a quench dilatometer at 450 °C for 10^5 s. To match the input format of the MC code, the EBSD data was transformed from a hexagonal to a square grid using Oxford

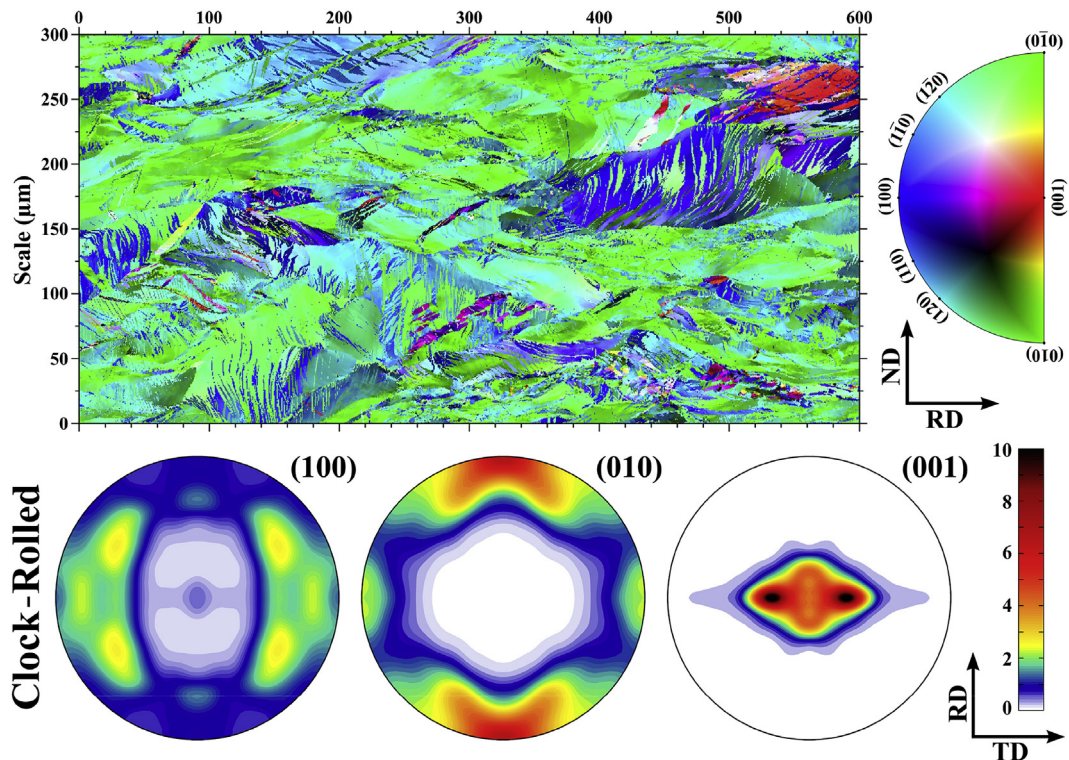


Fig. 1. Experimental EBSD map and stereographic pole figures of the α -uranium warm clock-rolled deformed microstructure adapted from data originally presented in Ref. [31], with inverse pole-figure (IPF) coloring along the RD direction. Inversion symmetry can reduce the IPF map further by half, but has not been applied to maintain contrast in the figure. The microstructure is dominated by multiple modes of deformation twinning and large intragranular misorientation gradients. There is a strong alignment of the (010) axes along the rolling direction, and the (001) axes along ND with a clear splitting along TD.

Instruments HKL Channel 5 software, with spatial aliasing during conversion acting as a high-pass filter. Analysis of experimental and simulated EBSD data was carried out using the MTEX MATLAB toolbox [65].

3. Computational methods

The simulations conducted for this paper were performed with a standard implementation of Potts MC code developed for grain growth simulations, outlined in Ref. [66], adapted to modeling recrystallization with modifications presented in Refs. [38–41]. This code has been made available with the article as open source *Supplementary material*. The most significant complication in adopting the standard Potts model to include recrystallization arises during scenarios where the neighboring site selected during an event has not yet recrystallized ($E_i > 0$). The dislocation network responsible for stored energy will not move along with the evolving grain boundaries in a deformed microstructure, and a grain boundary moving through a site will clear it of its existing dislocations (setting $E_i = 0$). As a consequence, any instance where a site is reassigned to the grain of a non-recrystallized neighboring site will create a new recrystallized nucleus via the bulge mechanism, a process typically limited to low-temperature or high-stress conditions [67]. To model recrystallization via site-saturated preexisting nuclei, as expected for α -uranium, the deformed sites in the simulation must be held static [39] and all events where the selected neighboring assignment belongs to a non-recrystallized grain terminated with no change to the microstructure.

When a Potts recrystallization model is initiated from experimental EBSD data, a scaling factor must be introduced between the boundary energy, γ_i , and the experimentally determined stored energy values, E_i , so that both are in commensurate units. As this scaling factor is difficult to calculate, it can be noted that in sufficiently deformed systems the stored strain energy is much larger than the interfacial energy ($E_i \gg \gamma_i$). In this limit, any event where a recrystallized grain expands into a deformed site has $\Delta H < 0$ and the release of stored energy always overcomes the creation of any new boundaries. This yields a particularly straightforward adaptation of the standard Potts model to the recrystallization process (under the assumption that the microstructure is heavily deformed); where a recrystallized grain will always expand into a deformed site if presented the opportunity, deformed sites are otherwise held static, and standard grain growth behavior can occur between recrystallized grains that have already impinged upon one another.

Due to differences in the driving forces behind recrystallization and standard grain growth, boundaries moving in response to recrystallization will have a considerably higher velocity. As a boundary is only able to travel one lattice site during a simulation event, differences in boundary velocity within Potts MC recrystallization simulations are accounted for statistically over a number of events by scaling the probability of each type of event succeeding. Given the speed at which recrystallization occurs in α -uranium at 450 °C [20], no curvature driven grain growth needs to occur during the simulation. Eliminating all grain growth events between recrystallized grains, however, produces ragged unphysical grain boundaries in the microstructure due to the statistical nature of the MC model. The grain growth probability (i.e. velocity) in this study was therefore reduced so that only one fifth of energetically successful attempts were allowed to proceed. This reduced probability proved sufficient to resolve the ragged boundaries between impinging grains, but was small enough to largely eliminate curvature driven grain growth (energetically favorable grain growth events occur infrequently along smooth

grain boundaries and are often returned to their original state in subsequent steps, producing slow net movement per time step relative to recrystallization events).

The recrystallization event success probability can be modified based on the stored energy released by the deformed site (ΔE_i) [38–40], as the velocity of a recrystallizing boundary will be proportional to the driving force [68]. Allowing recrystallized grains to expand into deformed sites with 100% probability (as done in this study) effectively fixes the velocity of the recrystallization boundaries to a constant and treats the deformed microstructure as a mean field, which is a reasonable approximation that can be refined as more experimental data becomes available. Comparing the number of simulation steps needed with the experimentally observed time to complete recrystallization [31] reveals that the recrystallization boundary velocity is expected to be approximately 5 nm/s, with 1 site = 0.5 μm and 1 time step ≈ 100 s. This is consistent with the largest recrystallized grains (which have grown with the least impingement) in the experimental microstructure reaching a maximum radius of 50 μm in 10,000 s (5 nm/s). For comparison, grain growth in α -uranium occurs at a rate of approximately 0.05 nm/s at 550 °C [69], and will be even more negligible at 450 °C.

The advantage of this simple form of the Potts recrystallization model (constant recrystallization velocity, negligible grain growth), illustrated in Fig. 2, is that predictions of recrystallization textures can be made without the need to first establish a large number of model parameters. Different criteria for assigning recrystallized nuclei within the deformed α -uranium microstructure were tested in an effort to find the best match to the experimental recrystallization texture. Recrystallization “nuclei” in a site-saturated model do not arise from a random thermally activated stochastic process; rather, they are already present within the microstructure as subgrains, supplying that the EBSD pattern is acquired with a suitable spatial resolution to capture them (after some recovery, as in the present study [31]). Designating nuclei as recrystallized in the model requires assigning an energy of $E_i = 0$ to the desired sites at the start of the simulation, allowing them to inherit the crystallographic orientation of the site in the deformed state [40]. The nucleation criterion that provides the closest match to the experimental recrystallization texture will identify the conditions that make a given sub-grain more likely than others in the microstructure to becoming a recrystallized nucleus.

Recrystallized nuclei often form preferentially at heterogeneities within a microstructure such as grain boundaries. Several nucleation conditions related to HAGBs were tested, e.g. including or excluding twin boundary sites. For the purposes of this paper, the definition of a HAGB was chosen as a boundary with misorientation >20°, as the deformed α -uranium microstructure exhibits considerable intragranular misorientations. Significant misorientation variations also occur along twin boundaries, so “twins” were categorized very simplistically as any boundary within a 60°–80° misorientation window. A map of HAGBs and twin boundaries, following this designation, is presented in Fig. 3. It can be seen that twin identification strategy is sufficient to correctly categorize most boundaries in the microstructure. A model refinement to handle twin identification would need to be adapted if that were not the case [70]. Grain boundary sites were defined as being separated from a minimum of two neighboring sites and no more than six by a qualifying misorientation angle; suppressing nucleation from experimental noise in the raw EBSD data.

Another set of nucleation conditions was employed to test whether nucleation occurs preferentially at points in the microstructure with large stored energies. For the purposes of this study, stored energy was determined by KAM values using a 3 × 3 grid with a 10° grain boundary threshold. This choice of KAM kernel

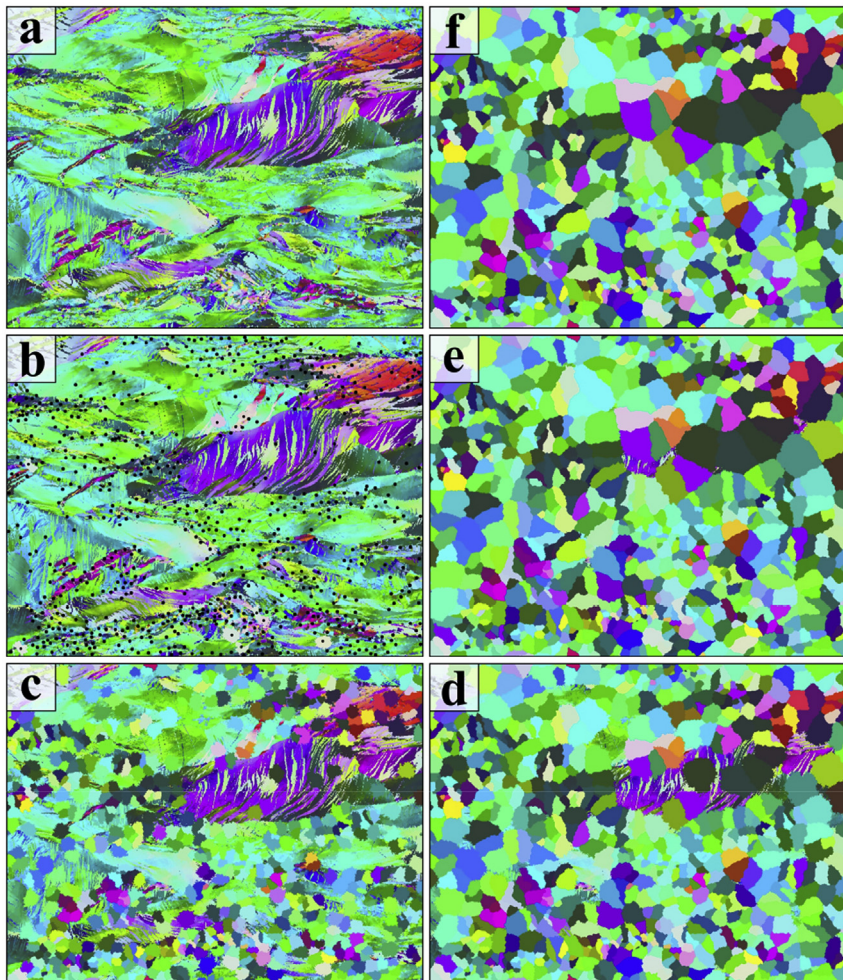


Fig. 2. Starting from an experimental EBSD map of the deformed microstructure (a), a set of recrystallized nuclei is assigned based upon a microstructural condition (b). Using a simple Potts MC model the recrystallized grains at first expand freely through the deformed microstructure (c) until impinging upon each other (d), at which point they become fixed with the exception of some gradual boundary smoothing due to a very limited grain growth term. The recrystallized grains continue to grow through the deformed structure (e) until the microstructure is fully recrystallized (f).

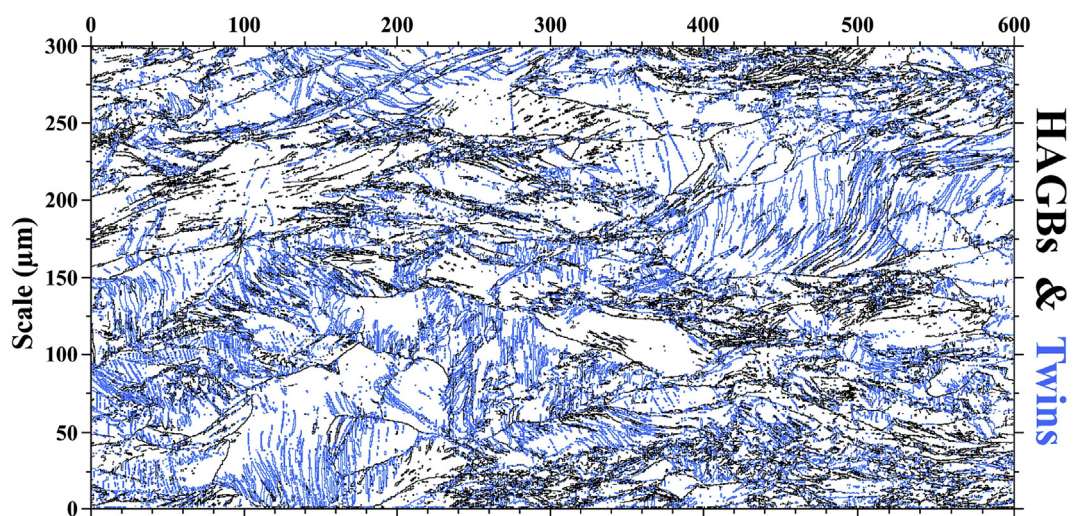


Fig. 3. Map of grain boundaries designated either as HAGBs or Twins for the α -uranium warm clock-rolled deformed microstructure seen in Fig. 1.

assumes the recrystallized nuclei are not larger than a single site (at the $0.5 \mu\text{m}$ step size), and focuses only on misorientation from the most immediate neighbors. The 10° threshold likely subsumes

some low angle grain boundaries into the KAM, but is necessary due to the degree of intragranular misorientation present in the microstructure. A KAM map of the deformed microstructure is

presented in Fig. 4. KAM values are heterogeneously distributed about the microstructure and several regions are comparatively low in deformation. Sites with the highest KAM tend to appear in clusters, strings, or bands located within areas of the deformed microstructure with a large number of non-twin HAGBs. The distribution of KAM values is approximately log-normal (Fig. 5). About 3.5% of sites in the deformed microstructure are calculated to have a KAM of 0, which occurs due to experimental noise creating points that have greater than 10° misorientation with all neighboring sites within the kernel. As recrystallized grains are defined by $E_i = 0$ for modeling purposes, these grains were assigned $E_i > 0$ to ensure that no unintentionally recrystallized sites were created. A probability function has been previously proposed for handling nucleation base on stored energy conditions in Potts recrystallization models:

$$n_i = 1 - \exp\left(-\frac{E_i - E_1}{E_2 - E_1}\right) \quad (2)$$

where E_1 is a threshold of stored energy that E_i must exceed for nucleation to take place, and E_2 is a parameter that controls the form of the function [39]. In the case that E_2 approaches E_1 , the nucleation probability reduces to a simple threshold. A simple threshold condition was utilized in this study because the available EBSD data is not large enough to meaningfully fit a set of both E_1 and E_2 parameters.

All simulated results presented in this paper were executed over 100 MC time steps unless otherwise noted, which was sufficient for the simulated microstructure to completely recrystallize. Three separate simulations were run at every nucleation condition and averaged to provide a representative crystallographic texture. Periodic boundary conditions were imposed to address lattice sites at the edges of the EBSD data, as the percentage of grains that contact the boundary at initialization is sufficiently small to reduce any associated artifacts. Orientation distribution functions were calculated from the experimental and simulated microstructures with a 5° angular resolution using the MTEX software package.

4. Results

The deformed microstructure of a warm clock-rolled α -uranium sample (Fig. 1) was used to initialize all of the simulations presented within this paper. Numerous thin and often serpentine deformation twins of several modes are present within most grains. Significant ($>10^\circ$) intra-granular misorientation gradients occur

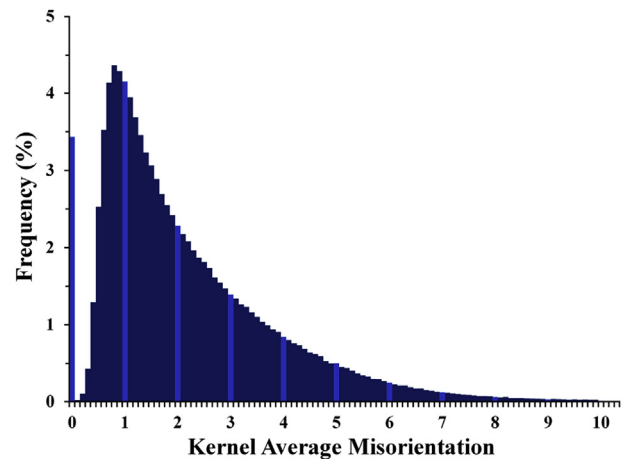


Fig. 5. Histogram of KAM values (3×3 grid, 10° threshold) for the α -uranium warm clock-rolled deformed microstructure seen in Fig. 1, exhibiting an approximately log-normal distribution.

within both the parent grains and twins. The map is orientated in the transverse direction (TD), and grains appear elongated along the rolling direction (RD). All crystallographic textures within the article are presented as pole figures with stereographic equal-angle projections in units of multiples of a random distribution (MRD), as much of the previous literature predates the invention of orientation distribution functions (ODFs). Complete ODFs for all of the textures can be found as *Supplementary material*. Due to the limited number of grains collected in an EBSD scan, the rolled plate's orthotropic symmetry has been imposed on the textures presented throughout this paper.

In order to unambiguously discuss the crystallographic texture, it is advantageous to introduce a graphical legend of distinct texture elements (*) that appear repeatedly between the deformed and recrystallized textures in both this study and the literature (Fig. 6). The crystallographic texture of warm clock-rolled uranium (Fig. 1) is characterized by a strong alignment of (010) poles along RD (*C, and the more diffuse *D), and collection of (001) poles near the normal direction (ND) with a clear splitting along TD (*G). If the texture were solely concentrated at elements *C in the (010) and *G in the (001) pole figures, geometry would dictate the presence of strong elements at *B in (100). Instead, *B is relatively weak compared to the stronger

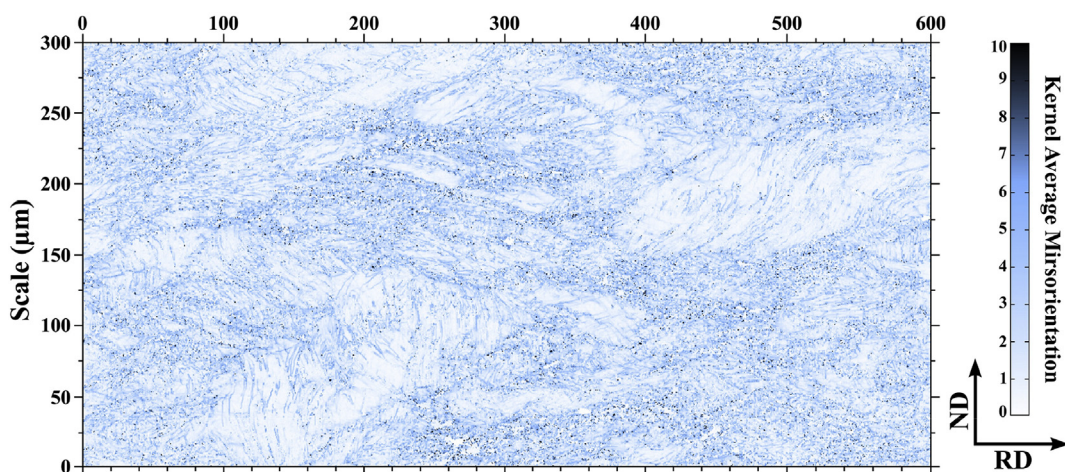


Fig. 4. Map of KAM values (3×3 grid, 10° threshold) for the α -uranium warm clock-rolled deformed microstructure seen in Fig. 1, showing heterogeneity between different regions.

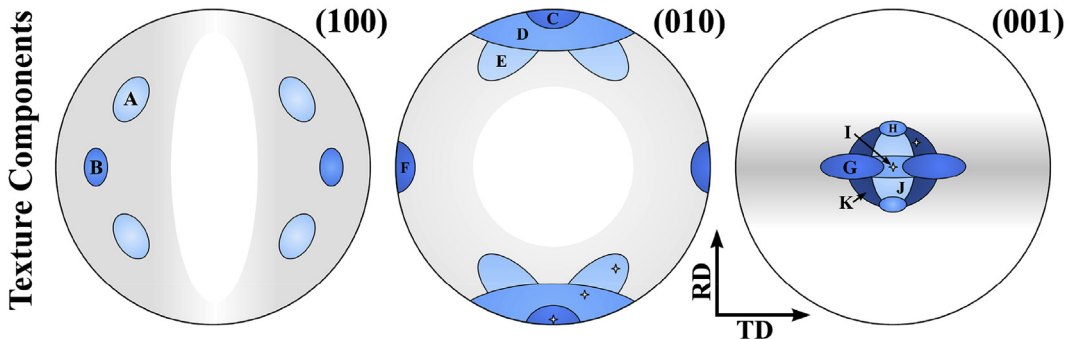


Fig. 6. Graphical legend of distinct texture elements (*) that appear repeatedly within the deformed and recrystallized α -uranium textures. The small crosses (+) in several of the elements mark representative locations used later in Fig. 9.

four-fold element *A in the (100) pole figure in the deformed state. These *A features correspond geometrically to the arm-like *E elements in the (010) pole figure, rotating about axes defined by the two very strong *G texture elements. Other features of note are a weak *F texture in the (010) pole figure, and a smooth, strong intensity across features *H–*K in (001).

For comparison, Fig. 7 presents an EBSD map of the clock-rolled material recrystallized at 450 °C for 10⁵ s and determined to be 91% transformed (with the remaining percentile being highly recovered) [31]. The deformation twins and intragranular misorientation gradients prevalent in the deformed microstructure have been replaced by a finer grained microstructure of relatively defect-free

grains. There is notable clustering of like-sized grains in bands along RD. This clustering is attributed to the inhomogeneous distribution of recrystallization nuclei in the deformed microstructure [31]. The observed texture agrees well with previously published textures for similar recrystallized warm clock-rolled material (50% reduction at 330 °C, recrystallization at 550 °C [7]). Overall the texture is considerably weaker than that of the deformed state. This is best observed in the (001) pole figure where the split TD texture (*G) drops from a maximum of 10 to 5 MRD, elements *H–*J disappear, and the intensity spreads outward in a diffuse halo across much of the pole figure. The ring-like *K element remains weakly present, strengthening where it connects the prominent *G

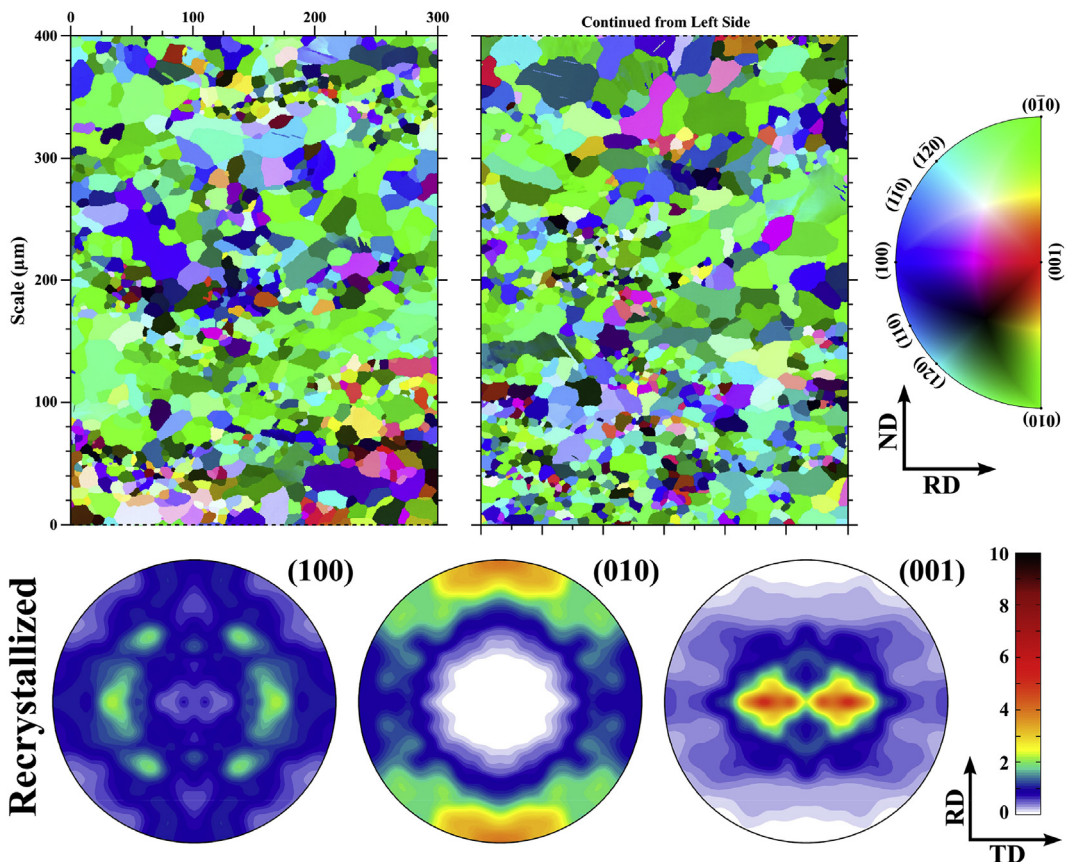


Fig. 7. Experimental EBSD map and stereographic pole figures of the α -uranium warm clock-rolled deformed microstructure recrystallized at 450 °C for 10⁵ s, originally presented in Ref. [31]. Inverse pole-figure (IPF) coloring is along the RD direction. The recrystallized grains are clustered into like-sized bands across the microstructure and the texture has evolved from the deformed state, becoming notably weaker.

elements. In the (010) pole figure, the axes remain preferentially oriented along the rolling direction, but the maximum intensity has weakened from 7 to 4 MRD, and the stronger *C element has disappeared into the more diffuse *D, while the arm-like *E extensions have retreated. With the loss of *E in the (010) pole figure, the associated *A elements of the (100) are much lower in intensity, while *B has maintained its original intensity and has become the strongest remaining feature. Both the *A and *B elements in the (100) pole figure, as well as the strong *G element in the (001), have experienced a geometrically correlated angular spread along the TD direction (rotating grain orientations about an axis defined by the (010) *C and *D elements along RD). Element *F has disappeared completely in the recrystallized microstructure.

The goal of this study was to identify sites in the deformed microstructure that are the most likely to form recrystallized nuclei, and thereby to discern factors influencing recrystallization in the α -uranium system. To identify these sites, a number of different assignment conditions were tested using the Potts recrystallization model; namely HAGBs sites excluding and including twin boundaries, sites with KAM above different threshold values, or combinations of these conditions. The simulated textures from these different nuclei assignments were then compared to the experimental recrystallization texture to

determine the closest match and any informative trends. For labeling purposes, the HAGB condition includes only the boundary sites designated as HAGBs in Fig. 3 (excluding twin boundaries), while the HAGB + Twins condition includes all of the boundary sites. For each condition nuclei were placed only at sites that simultaneously satisfied all applicable conditions related to the location of grain boundaries (Fig. 3) and their KAM values (Fig. 4). The number of nuclei assigned per simulation in the presented work was held constant at ~1200, regardless of the nucleation conditions, by applying a probability of success to each nucleation site based upon the total number of qualifying nuclei. This cap is the approximate number of nuclei needed to reproduce the observed experimental recrystallized grain size, and also matches the number of nuclei found in the condition that provided the best texture prediction.

It was hypothesized in the original EBSD study that recrystallized nuclei form along non-twin HAGBs in the deformed microstructure at 450 °C [31]. The closest match to the experimental crystallographic texture (over an entire microstructure) occurs when the selected nuclei are non-twin HAGB sites with $KAM > 9$, suggesting that nucleation does not occur homogeneously along these boundaries. The simulated textures from a selection of the explored nucleation conditions are compared in Fig. 8. Each of

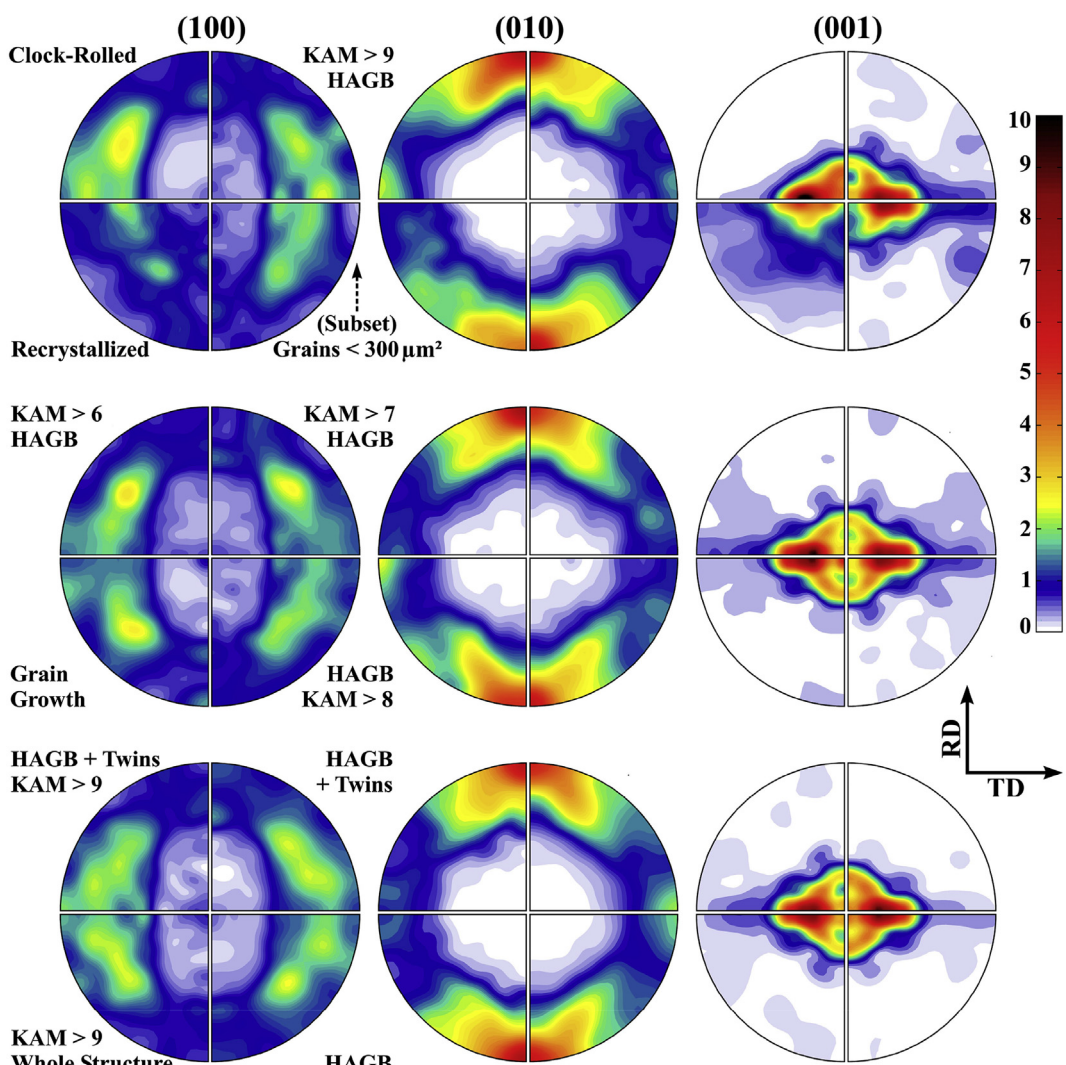


Fig. 8. Simulated EBSD stereographic pole figures for a number of recrystallized nuclei conditions, along with the experimental clock-rolled and recrystallized textures. The pole figures have been reduced to show only a fundamental quadrant, applying the rolled sample's orthotropic symmetry.

these conditions will be discussed in the following paragraphs. Difference pole figures from the experimental recrystallized texture can be found as *Supplementary material* for all conditions. To aide in interpretation of Fig. 8, Fig. 9 graphically displays the strength of the distinct texture elements identified in Fig. 6 for each of the pole figures. Depending on the texture element, the MRD values in Fig. 9 are either the maximum (*A, *B, *F, *G, *H) or minimum (*J) found within each element, or the value at a specific representative location (*C, *D, *E, *I, *K) marked in Fig. 6. It is important to note the size and importance of each element is not equal, and these numbers do not capture changes in the spread or shape of the elements that are best observed in the pole figures themselves. Nonetheless, this semi-quantitative chart helps to visualize related trends and variations between the many pole figures.

The HAGB: KAM >9 condition for recrystallized nuclei (Fig. 10) is able to replicate many of the differences experimentally observed between the deformed and recrystallized textures. In the (010) pole figure element *F has disappeared, both the *C and *D elements in (010) have weakened from the deformation texture, and the arm-like *E extensions are less prominent than in the deformed state. The primary difference between the simulated and experimental (010) pole figures is the concentration of intensity directly along RD (*C) rather than being spread across the broader *D element. As with the experimental texture, the loss of *E in the (010) pole figure has led to a corresponding decrease in the associated *A elements of the (100) figure, leaving *B as the strongest remaining feature. Larger disparities occur in the (001) pole figure, despite the simulated and experimental textures undergoing a qualitatively similar evolution. The strong *G texture of the deformed microstructure remains the most intense element and has decreased in intensity, but not by the same extent as the experimental observation. Elements *H-*K have lost significant portions of their original

intensity, but unlike the experimental texture, they have not completely disappeared.

The simulated microstructure in Fig. 10 produces the clustering of grains of similar size seen in the experimental microstructure (Fig. 7). This clustering arises from a heterogeneous density of recrystallized nuclei within the deformed microstructure. Larger recrystallized grains are located in regions of lower deformation (Fig. 4), as the lower density of resulting nuclei will not impinge upon each other immediately during growth (Fig. 2). Conversely, regions with smaller grain sizes correspond to areas of greater initial deformation, where the density of nuclei is higher and there is little room for each nucleus to grow. Histograms of the experimentally measured and simulated grain sizes both exhibit log-normal distributions, but the mean grain size of the simulated microstructure is larger ($164 \mu\text{m}^2$) than that of the experimental ($100 \mu\text{m}^2$). Differences in the grain size distributions are consistent with effects introduced by limiting the simulation to 2D. In a 3D microstructure grains nucleated above and below the 2D plane will result in a smaller cross-sectional area per grain for a given density of nuclei (per voxel). While modeling 3D microstructures would offer improvements, the intensive characterization needed to acquire such data is not always feasible. Inference methods to extrapolate 3D microstructures from 2D EBSD maps exist, but are designed to handle single orientation grains (without intragranular misorientations) [71]. 2D simulations remain an efficient means for studying phenomena and establishing support for experimentally verified trends.

Relaxing the HAGB: KAM >9 condition to include twin boundary sites or all points in the microstructure with KAM >9 produces two nearly-identical simulated textures, both of which are similar to the HAGB: KAM >9 condition. This is because nearly all sites with KAM >9 occur along boundaries within the microstructure, so removing

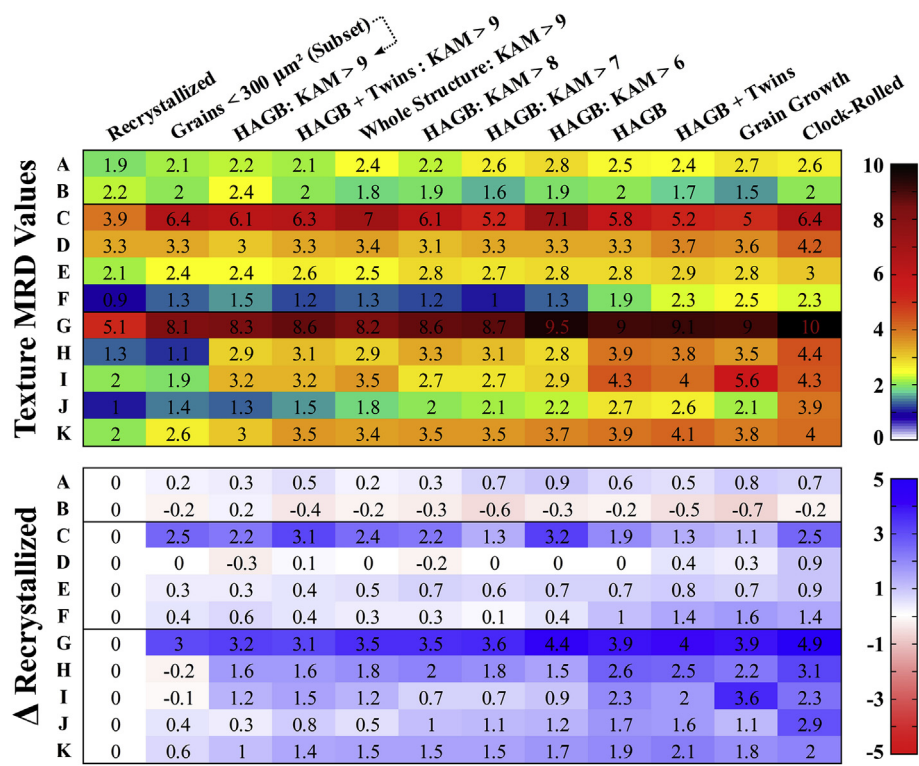


Fig. 9. Trends in the strength of the different elements (Fig. 6) between both experimentally determined and simulated recrystallization textures found in Fig. 8. Note: The importance of each element is not equal and the values do not always capture changes to the spread or shape of the elements, which are better observed in their respective pole figures.

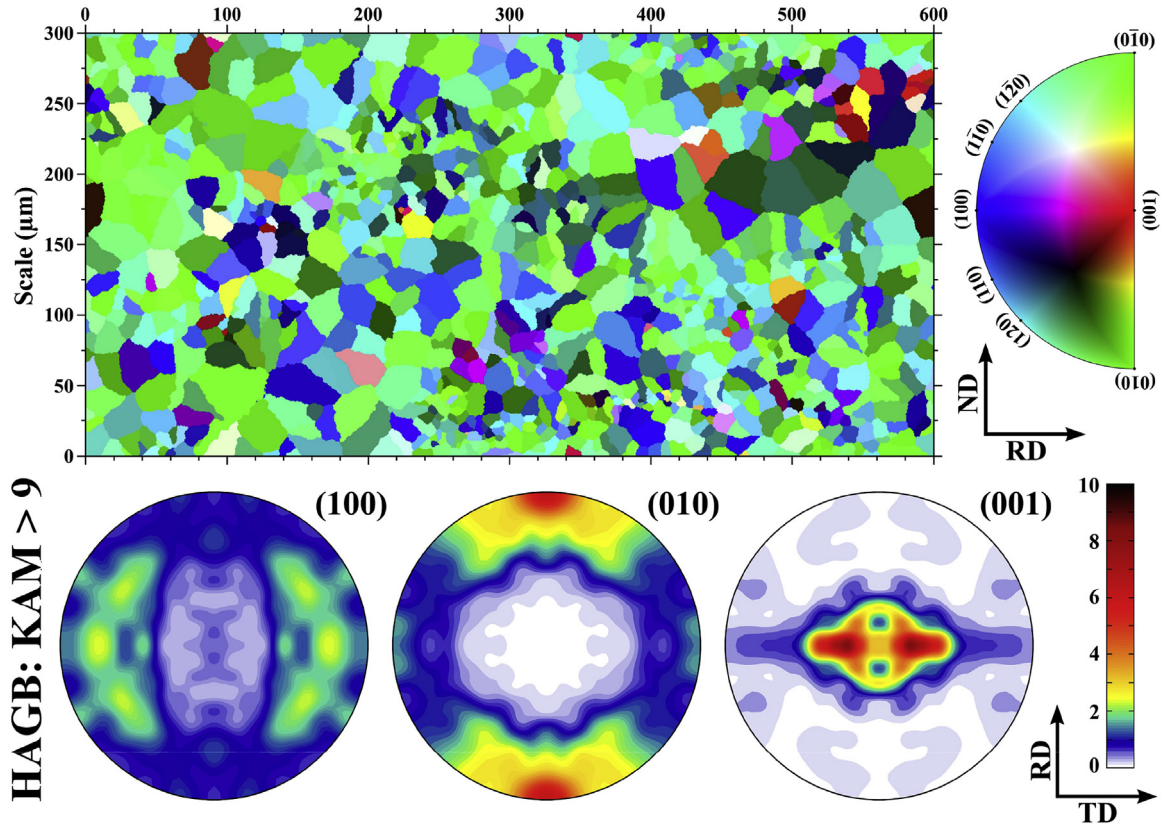


Fig. 10. Simulated EBSD map and stereographic pole figures of a recrystallized α -uranium warm clock-rolled microstructure, with inverse pole-figure (IPF) coloring along the RD direction. This figure was generated starting from the microstructure in Fig. 1 and employing the Potts MC recrystallization model, with recrystallized nuclei set as all points along non-twin HAGBs with KAM >9.

the grain boundary requirement makes little difference. The two alternative KAM >9 conditions both have textures with weaker *B elements relative to HAGB: KAM >9, stronger *D elements, and *J and *K elements that have not reduced to the same extent. All of the KAM >9 conditions, however, are able to replicate the most notable evolutions from the deformed microstructure: weakening of all elements in the (010) and (001) pole figures, including the near disappearance of *F and *J, and the retreat of elements *E and *A in favor of *B. The importance of including a KAM nucleation condition is highlighted by the textures simulated using only boundary conditions, HAGB or HAGB + Twins. In both of these cases all the elements of the (001) poles are nearly unchanged from the deformed state, suggesting the original hypothesis in Ref. [31] was incomplete. The *E element of the (010) pole figure remains pronounced, and the *F element that disappears experimentally remains close to its original strength. The (100) *B element becomes weaker than even the deformed state. Thus, nucleation using only HAGB conditions is unable to fully account for all aspects of the observed texture evolution in α -uranium during recrystallization. The inclusion or exclusion of twin boundaries as potential nucleation sites results in relatively subtle variations in the simulated textures.

Maintaining the non-twin HAGB condition and adjusting the KAM threshold to different values, it can be seen that the KAM >9 threshold provides the closest texture to the experimental result. With increasing KAM thresholds, the prominent *G, *J and *K elements of the (001) pole figure steadily reduce in spread and intensity, while the relatively minor *I and *H elements exhibit no clear trend. All threshold conditions below KAM >9 exhibit stronger *E and *D elements in (010) than the KAM >9 condition. With

decreasing KAM thresholds, the *A element of the (100) grows increasingly prominent and exhibits less spread. Finally, applying pure grain growth modeling in the absence of recrystallization to the microstructure and running the simulation until reaching a comparable grain size (600 MC time steps) results in a texture that is similar to the HAGB + Twins condition, with the exception of a stronger *I and weaker *J element in the (001) pole figure. All of these trends support the conclusion that grain boundary sites with the highest KAM values serve as recrystallization nuclei.

5. Discussion

Textures simulated by nucleation along non-twin HAGBs in the deformed α -uranium microstructure approach the experimental recrystallization texture as previously hypothesized [31], but only through identification of preferential sites with large stored energies (KAM > 9). KAM thresholding appears to be a more important condition to identifying nucleation sites than the presence of a HAGB, as the textures generated using only a KAM >9 threshold are closer to the experimental texture than those generated using only the HAGB condition. This is partly due to the fact that KAM >9 sites exist almost exclusively as a subset HAGB sites, so the condition cannot be isolated. While the simulated results are able to capture a large portion of the α -uranium recrystallization behavior, failure of the simulated recrystallization texture (Fig. 10) to completely replicate the experimental texture (Fig. 7) suggests that improvements can still be made to the model.

One major difference remaining between the simulated and experimental textures is the continued presence of the *H, *I and *K elements of the (001) pole figure. By separating the simulated

HAGB: KAM >9 texture into contributions provided by recrystallized grains of difference sizes, it is clear that the *H , *I and *K elements originate from only the largest ~15% of grains in the microstructure (Fig. 11, Grains $>300 \mu\text{m}^2$), which make up about half the areal fraction. Large grains in the simulation form as clusters within the least deformed regions, where a low density of recrystallized nuclei allows for the few existing nuclei to expand significantly before impinging upon each other. Failure of the simulation to capture the experimentally observed disappearance of the *H , *I and *K elements may originate from the misidentification of some sites in these regions as recrystallized nuclei and their subsequent disproportionate growth. Close inspection of KAM values (Fig. 4) shows isolated points with KAM >9 occasionally occur in regions of otherwise low deformation where twins of different modes or variants cross each other, and are likely the primary source of such spurious nucleation sites. Replacing the constant recrystallization boundary velocity with a version scaled by the stored energy released, as discussed in the previous section, could help suppress the contribution of the larger grains in the current simulation, as their nuclei are located within regions of low deformation where the recrystallized grains would expand more slowly. A 3D initial dataset could also rectify the problem by providing correctly identified nucleation sites above and below the 2D plane of the present section, so that those coinciding with regions of low deformation have potential to supplant nuclei with the incorrect texture. Given the difficulty of acquiring detailed experimental 3D microstructures including a stored energy parameter, the exact impact of moving from 2D between 3D will likely need to be studied using simulated deformed microstructures.

In the absence of the larger grains, the remainder of the simulated microstructure comprised of 85% of the grains (Fig. 11, Grains $<300 \mu\text{m}^2$) is close to the experimental recrystallization texture. The only remaining difference is the predominant *C and *G elements of the texture remain approximately 60% more intense than expected. Texture strength can be expressed quantitatively as a texture index (J_{ODF}) that will take the value of 1 at complete randomization, and infinity for a perfect single crystal [72]. The deformed microstructure (Fig. 1) has a texture index of 5.9, which weakens to a recrystallized state of 2.6 (Fig. 7). For comparison the HAGB: KAM >9 texture (Fig. 10) has a value of 4.3, and the Grains $<300 \mu\text{m}^2$ subset has a value of 4.1. None of the nucleation conditions tested were able to match the degree of randomization observed experimentally. This is because the simulation currently selects recrystallized grain orientations from a sub-set of the orientations present in the deformed microstructure. As there are few grains oriented significantly away from ND in the (001) pole figure

in the deformed microstructure, it is impossible for those orientations to appear during the simulation. One possibility is that the EBSD map was not acquired at a sufficient resolution to capture all of the possible sub-grain orientations that would later become nuclei, and that it systematically failed to identify sub-grains with more random orientations.

Another possibility is that the deformation microstructure in Fig. 1 has not completed recovery and that the dislocation walls that separate sub-grains are still forming. In order to acquire a well-indexed EBSD pattern, the deformation microstructure was annealed at 450 °C for 30 s prior to analysis [31], which was believed to be sufficient for dislocations to form a recovery microstructure and establish sub-grain boundaries. Due to the complexity of deformation modes in α -uranium, and the large intra-granular misorientations still present in Fig. 1, this assumption may be incorrect. If dislocations continue to rearrange prior to recrystallization, a broader spread of site orientations than observed in Fig. 1 could be formed. The deformation modes active in α -uranium are complex and highly dependent on temperature and nature of the applied stress [5–10]. Warm clock-rolling at 300 °C is expected to result in high activity of the [100](010), [100](001) and $\frac{1}{2}\bar{1}\bar{1}0\{110\}$ slip modes, in addition to deformation twinning. A tilt wall sub-grain boundary formed by [100](001) “floor” mode dislocations will rotate the c-axis of the material forming a sub-grain in the c-a plane about the b-axis. For the texture of clock-rolled α -uranium, with a strong alignment of the (010) axis along RD, evolving floor mode tilt boundaries would therefore lead to the experimentally observed spread of *G elements in the (001) pole figure along TD. Tilt walls of the [100](010) “wall” and $\frac{1}{2}\bar{1}\bar{1}0\{110\}$ “chimney” modes would both result in analogous rotations about the c-axis and spreading of the *C element away from RD. Through these mechanisms it is possible that the nucleation sites identified in the model would experience rotation away from the strong *C and *G features before the onset recrystallization as their sub-grain boundaries form, explaining the observed differences between the experimental recrystallization texture (Fig. 7) and the simulated recrystallization texture (Fig. 11, Grains $<300 \mu\text{m}^2$). It is important to note that this potential mechanism, involving the formation of sub-grains during recovery and their rotations from the deformed parent grain matrix, is distinct from continuous sub-grain rotation during dynamic recrystallization. None of the possible explanations for why the model fails to capture the randomization is exclusive and further work exploring the effects of EBSD scan resolution and recovery times will be needed to sort out their relative contributions.

Recrystallization textures in α -uranium are expected to be

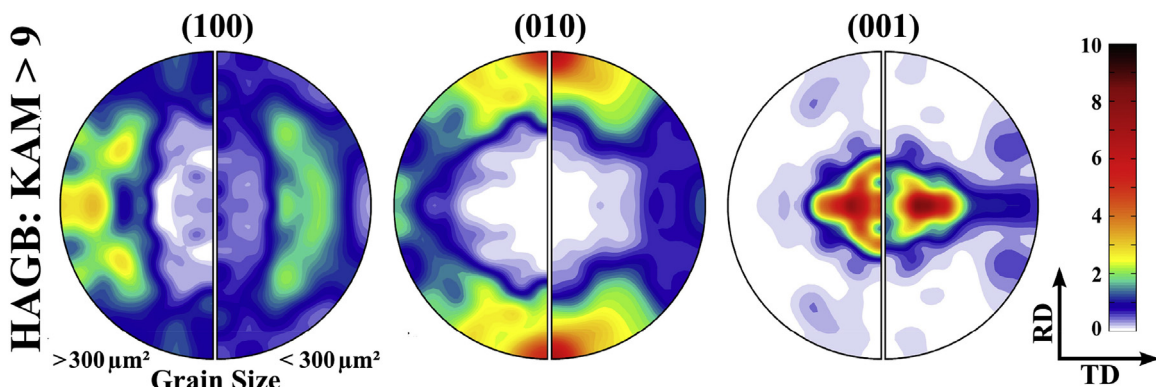


Fig. 11. Simulated EBSD stereographic pole figures for the recrystallized α -uranium warm clock-rolled texture in Fig. 10 (HAGB: KAM > 9) broken out into sub-textures for Grains $> 300 \mu\text{m}^2$ and Grains $< 300 \mu\text{m}^2$.

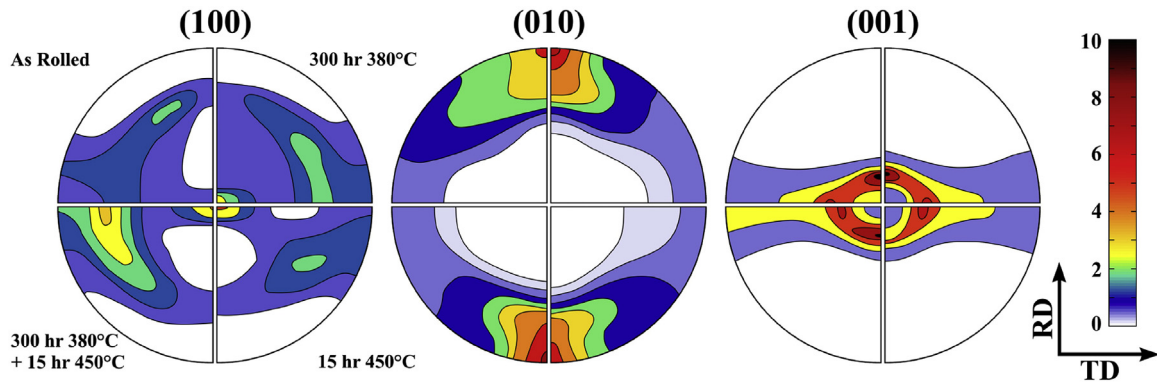


Fig. 12. Experimental XRD stereographic pole figures of straight cold-rolled α -uranium and recrystallization textures at different heat treatment conditions, adapted from raw data presented in Ref. [20] and converted into approximate MRD scale values for comparison.

temperature dependent, based upon prior results obtained on material which was cold straight-rolled (at room temperature) and recrystallized using a range of different heat treatments (Fig. 12) [20]. As a consequence, care must be taken when extrapolating some results presented in this paper to other temperature ranges. The deformation texture of cold straight-rolled α -uranium is relatively close to the warm clock-rolled texture, with strong alignment of (010) along RD, a four-fold *A element in (100), and a split TD *G element in (001). Where the warm clock-rolled deformation texture has equally strong intensity along elements *H-K, the cold straight-rolled texture has a very prominent *H element, moderate *K, and notably weaker *I and *J elements. Recrystallization at 380 °C (300 h) results in only minor evolution in the texture, primarily weakening of the *I and *J elements and appearance of the *B element. In stark contrast, recrystallization at 450 °C (15 h) results in the complete disappearance of the strong *H element along with *I and *J, in a comparable trend to the warm clock-rolled recrystallization texture at 450 °C. To ensure the difference observed between 380 °C and 450 °C did not result from texture evolution during grain growth, samples recrystallized at 380 °C were subsequently subjected to a 450 °C grain growth treatment, producing a stronger *B element but few other changes. There are at least two possible explanations for the temperature dependency of the α -uranium recrystallization texture. Recrystallization at lower temperatures over longer times is likely to result in a greater density of nuclei forming within the microstructure, which likely means nucleation on HAGBs in the deformed microstructure at 450 °C. These nuclei do not occur homogeneously along the HAGBs, however, and are preferentially located in areas of large stored energy, indicated by especially high intra-granular misorientations measured using Kernel Average Misorientation (KAM) values. Additionally, the strong temperature dependence of several hard slip systems in α -uranium, e.g. the $\frac{1}{2}1\bar{1}0\{110\}$ chimney mode, means that the recovery microstructure may vary significantly with temperature and alter the orientation of sub-grains that go on to form nuclei. If the contribution from the number density of nuclei is dominant, lower temperature recrystallization textures of warm clock-rolled samples should resemble the HAGB: KAM >6 or KAM >7 conditions, producing a stronger *A texture and weaker *B. Conversely, if sub-grain boundary evolution plays a large role, a texture that does not fit the KAM threshold based trend should be observed. Recrystallization of warm rolled α -uranium at temperatures at 550 °C [7] produces a similar texture to 450 °C, so recrystallization experiments at lower temperatures and longer times are necessary to establish the temperature dependency on crystallographic texture.

As crystal plasticity computational techniques have started to successfully predict α -uranium deformation microstructures [11,12,73], one of the remaining hurdles to simulating the full thermomechanical history of uranium components is developing an improved understanding of nucleation processes within the

material. It is here that results from Potts modeling used in conjunction with experimental EBSD data are able to provide a key contribution, by identifying conditions within the microstructure at different temperatures and deformation conditions that are most likely to form recrystallization nuclei. These conditions can then be incorporated into microstructural simulations to extend them through recrystallization processes and predict final microstructures, similar to Radhakrishnan et al. [41]. 85% of the nuclei identified by the HAGB: KAM >9 condition appear to have the correct recrystallization texture, and it is possible that the remaining 15% are mistakenly identified due to sources of experimental error that will not be present within a simulated microstructure. The application of Potts MC recrystallization models to EBSD data to screen for preferential nucleation conditions within the microstructure also has potential to help elucidate issues pertaining to the origination of the so called “rare-earth” texture in Mg-RE, Mg-RE-Zn, and Mg-Ca-Zn alloys, which currently remains unresolved [74].

6. Conclusions

A Monte Carlo Potts model was used to simulate static recrystallization textures resulting from annealing of warm clock-rolled α -uranium. Different nucleation site selection concepts applied to experimental EBSD data revealed that nuclei form, as previously hypothesized, along non-twin HAGBs in the deformed microstructure at 450 °C. These nuclei do not occur homogeneously along the HAGBs, however, and are preferentially located in areas of large stored energy, indicated by especially high intra-granular misorientations measured using Kernel Average Misorientation (KAM) values. In the future, trends noted between the choice of recrystallized nuclei within the deformed microstructure and the resulting simulated textures can in turn be applied to studies addressing the temperature dependency of α -uranium recrystallization textures. Pinpointing the microstructural conditions that can be used to best identify nuclei within α -uranium can inform how deformation microstructures simulated using crystal plasticity techniques will respond to recrystallization.

Acknowledgements

Funding for this research was provided by the Y-12 National Security Complex under the Plant Directed Research, Development, and Demonstration program. This work of authorship and those incorporated herein were prepared by Consolidated Nuclear Security, LLC (CNS) as accounts of work sponsored by an agency of the United States Government under Contract DE NA 0001942. Neither the United States Government nor any agency thereof, nor CNS, nor

any of their employees, makes any warranty, express or implied, or assumes any legal liability or responsibility to any non-governmental recipient hereof for the accuracy, completeness, use made, or usefulness of any information, apparatus, product, or process disclosed, or represents that its use would not infringe privately owned rights. Reference herein to any specific commercial product, process, or service by trade name, trademark, manufacturer, or otherwise, does not necessarily constitute or imply its endorsement, recommendation, or favoring by the United States Government or any agency or contractor thereof, or by CNS. The views and opinions of authors expressed herein do not necessarily state or reflect those of the United States Government or any agency or contractor (other than the authors) thereof. This document has been authored by Consolidated Nuclear Security, LLC, under Contract DE NA 0001942 with the U.S. Department of Energy/National Nuclear Security Administration, or a subcontractor thereof. The United States Government retains and the publisher, by accepting the document for publication, acknowledges that the United States Government retains a nonexclusive, paid up, irrevocable, worldwide license to publish or reproduce the published form of this document, prepare derivative works, distribute copies to the public, and perform publicly and display publicly, or allow others to do so, for United States Government purposes. Work performed at Los Alamos National Laboratory is supported by the Los Alamos National Laboratory Directed Research and Development (LDRD) project 20140630 ER. Los Alamos National Laboratory is operated by Los Alamos National Security LLC under DOE Contract DE-AC52-06NA25396. Electron microscopy was performed at the Los Alamos Electron Microscopy Laboratory.

Appendix A. Supplementary data

Supplementary data related to this article can be found at <http://dx.doi.org/10.1016/j.jnucmat.2017.04.026>.

References

- [1] J.E. Burke, A.M. Turkalo, The growth of Uranium upon thermal cycling, *Trans. ASM* 50 (1957) 943–953.
- [2] F. Foote, Physical metallurgy of uranium, in: *Progress in NuclearEnergy, Series V, Metallurgy and Fuels*, McGraw-Hill, New York, 1956, pp. 81–201.
- [3] R. Anderson, D. Carpenter, T. Kollie, D. Smith, Texture-property relationships in the uranium-2.4 weight percent niobium alloy, in: *Metallurgical Technology of Uranium and Uranium Alloys*, American Society for Metals, Metals Park, OH, 1982, pp. 231–249.
- [4] O. Sherby, D. Bly, D. Wood, Plastic flow and strength of uranium and its alloys, in: *Physical Metallurgy of Uranium Alloys*, Brook Hill Publishing Co, Chestnut Hill, MA, 1976, pp. 311–348.
- [5] D. Brown, M. Bourke, B. Clausen, R. Korzekwa, R. McCabe, T. Sisneros, D. Teter, Temperature and direction dependence of internal strain and texture evolution during deformation of uranium, *Mater. Sci. Eng. A* 512 (2009) 67–75.
- [6] R. McCabe, L. Capolungo, Marshall, C. Cady, C. Tomé, Deformation of wrought uranium: experiments and modeling, *Acta Mater.* 58 (2010) 5447–5459.
- [7] M. Knezevic, L. Capolungo, C. Tome, R. Lebensohn, D. Alexander, B. Mihaila, R. McCabe, Anisotropic stress-strain response and microstructure evolution of textured α -uranium, *Acta Mater.* 60 (2012) 702–705.
- [8] M. Knezevic, R. McCabe, R. Lebensohn, C. Tome, C. Liu, M. Lovato, B. Mihaila, Integration of self-consistent polycrystal plasticity with dislocation density based hardening laws within an implicit finite element framework: application to low-symmetry metals, *J. Mech. Phys. Solids* 61 (2013) 2034–2046.
- [9] M. Knezevic, R. McCabe, C. Tome, R. Lebensohn, S. Chen, C. Cady, G.G.III, B. Mihaila, Modeling mechanical response and texture evolution of α -uranium as a function of strain rate and temperature using polycrystal plasticity, *Int. J. Plast.* 43 (2013) 70–84.
- [10] C. Calhoun, E. Garlea, R. Mulay, T. Sisneros, S. Agnew, Investigation of the effect of thermal residual stresses on deformation of α -uranium through neutron diffraction measurements and crystal plasticity modeling, *Acta Mater.* 85 (2015) 168–179.
- [11] M. Zecevic, M. Knezevic, I.J. Beyerlein, R.J. McCabe, Origin of texture development in orthorhombic uranium, *Mater. Sci. Eng. A* 665 (2016) 108–124.
- [12] M. Zecevic, M. Knezevic, I.J. Beyerlein, R.J. McCabe, Texture formation in orthorhombic alpha-uranium under simple compression and rolling to high strains, *J. Nucl. Mater.* 473 (2016) 143–156.
- [13] R. Doherty, D. Hughes, F. Humphreys, J. Jonas, D. Jensen, M. Kassner, W. King, T. McNeley, H. McQueen, A. Rollett, Current issues in recrystallization: a review, *Mater. Sci. Eng. A* 238 (1997) 219–274.
- [14] R. Doherty, *Recrystallization of Metallic Materials*, Verlag, Berlin, 1978.
- [15] F. Humphreys, M. Hatherly, *Recrystallization and Related Annealing Phenomena*, Pergamon Press, Oxford, 1995.
- [16] R.D. Doherty, Recrystallization and texture, *Prog. Mater. Sci.* 42 (1997) 39–58.
- [17] A. Rollett, Overview of modeling and simulation of recrystallization, *Prog. Mater. Sci.* 42 (1997) 79–99.
- [18] R. Cahn, Plastic deformation of alpha-uranium; twinning and slip, *Acta Mater.* 1 (1953) 49–70.
- [19] M. Yoo, Slip modes of alpha uranium, *J. Nucl. Mater.* 26 (1968) 307–318.
- [20] L.T. Lloyd, M.H. Mueller, *Recrystallization in Rolled Uranium Sheet*, ANL-63Z7, Argonne National Laboratory, Argonne, Illinois, 1962.
- [21] M. Mueller, H. Knott, Preferred Orientation in Rolled and in Recrystallized High-purity Uranium, ANL-5887, Argonne National Laboratory, Lemont, Illinois, 1959.
- [22] E.C. Miller, W.H. Bridges, Metallurgy Division Quarterly Progress Report for Period Ending July 31, 1951, Oak Ridge National Laboratory, Oak Ridge, Tennessee, 1952.
- [23] N.D. Libanati, D. Calais, Lacombe, Recristallisation secondaire et recristallisation après écoulement critique de l'uranium de haute pureté, *J. Nucl. Mater.* 10 (1963) 23–42.
- [24] W.R. McDonell, Preferred Orientation of Cold-rolled and Recrystallized Uranium Plate, DP-258, Savannah River Laboratory, Aiken, South Carolina, 1957.
- [25] G.Y. Sergeev, V.T. Kolonneva, Recrystallization of cold-rolled uranium, *J. Nucl. Energy Parts A/B React. Sci. Technol.* 17 (1963) 444–447.
- [26] P. Madsen, The behavior of interfaces in lightly worked uranium during recrystallization, *J. Inst. Metals* 85 (1956) 71–75.
- [27] W. Chernock, A. Beck, Quantitative Determination of Rolling and Recrystallization Textures in 600C and 300C Rolled Uranium Rods, U.S. Atomic Energy Commission, Technical Information Service, Oak Ridge, TN, 1955.
- [28] J. Bingert, R.J. Hanrahan, R. Field, Dickerson, Microtextural investigation of hydrided alpha-uranium, *J. Alloys Compd.* 365 (2004) 138–148.
- [29] D. Carpenter, J. Bullock, OIM and EDX determination of the orientation dependence of corrosion in uranium metal, *Inst. Phys. Conf. Ser.* 165 (2000) 209–210.
- [30] R. McCabe, D. Teter, Analysis of recrystallized volume fractions in uranium using electron backscatter diffraction, *J. Microsc.* 223 (2006) 33–39.
- [31] R. McCabe, A. Richards, D. Coughlin, K. Clarke, I. Beyerlein, M. Knezevic, Microstructure effects on the recrystallization of low-symmetry alpha-uranium, *J. Nucl. Mater.* 465 (2015) 189–195.
- [32] H. Hallberg, Approaches to modeling of recrystallization, *Metals* 1 (2011) 16–48.
- [33] K.G.F. Janssens, D. Raabe, E. Kozechnik, M. Miodownik, B. Nestler, *Computational Materials Engineering*, Elsevier Academic Press, 2007.
- [34] M. Miodownik, A review of microstructural computer models used to simulate grain growth and recrystallisation in aluminium alloys, *J. Light Metals* 2 (2002) 125–135.
- [35] M. Miodownik, Monte carlo Potts model, in: *Computational Materials Engineering*, Elsevier Academic Press, 2007.
- [36] S.K. Esche, Monte Carlo simulations of grain growth in metals, in: M. Shlomo, S. Mordechai (Eds.), *Applications of Monte Carlo Method in Science and Engineering*, InTech, 2011.
- [37] F. Wu, The Potts model, *Rev. Mod. Phys.* 54 (1982) 235.
- [38] E. Holm, M. Miodownik, A. Rollett, On abnormal subgrain growth and the origin of recrystallization nuclei, *Acta Mater.* 52 (2003) 2701.
- [39] D. Solas, C. Tome, O. Engler, H. Wenk, Deformation and recrystallization of hexagonal metals: modeling and experimental results for zinc, *Acta Mater.* 49 (2001) 3791–3801.
- [40] Y. Chun, S. Semiatin, S. Hwang, Monte Carlo modeling of microstructure evolution during the static recrystallization of cold-rolled, commercial-purity titanium, *Acta Mater.* 54 (2006) 3673–3689.
- [41] B. Radhakrishnan, S. G. B. T. Zacharia, Modeling the kinetics and microstructural evolution during static recrystallization—Monte Carlo simulation of recrystallization, *Acta Mater.* 46 (1998) 4415–4433.
- [42] W. Read, W. Shockley, Dislocation models of crystal grain boundaries, *Phys. Rev.* 78 (1950) 275.
- [43] W. Shockley, W. Read, Quantitative predictions from dislocation models of crystal grain boundaries, *Phys. Rev.* 75 (1949) 692.
- [44] R.A. Lebensohn, N-site modeling of a 3D viscoplastic polycrystal using fast Fourier transform, *Acta Mater.* 49 (2001) 2723–2737.
- [45] E. Woldt, D. Juul Jensen, Recrystallization kinetics in copper: comparison between techniques, *Metall. Mater. Trans. A* 26 (1995) 1717–1724.
- [46] M. Black, R. Higginson, An investigation into the use of elec-tron back scattered diffraction to measure recrystallised fraction, *Scr. Mater.* 41 (1999) 125–129.
- [47] J. Tarasiuk, Gerber, B. Bacroid, Estimation of recrystallized volume fraction from EBSD data, *Acta Mater.* 50 (2002) 1467–1477.
- [48] F. Caleyo, T. Baudin, R. Penelle, Study of the development of thecube texture in Fe-50% Ni during recrystallization and normal grain growth, *Eur. Phys. J. Appl. Phys.* 20 (2002) 77–89.
- [49] D. Dingley, Progressive steps in the development of electron back-scatter diffraction and orientation imaging microscopy, *J. Microsc.* 213 (2004) 214–224.

- [50] W. Wang, A. Helbert, F. Brisset, M. Mathon, T. Baudin, Monte Carlo simulation of primary recrystallization, *Acta Mater.* 81 (2014) 457–468.
- [51] M. Calcagnotto, D. Ponge, E. Demir, D. Raabe, Orientation gradients and geometrically necessary dislocations in ultrafine grained dual-phase steels studied by 2D and 3D EBSD, *Mater. Sci. Eng. A* 527 (2010) 2738–2746.
- [52] D. Field, Trivedi, S. Wright, M. Kumar, Analysis of local orientation gradients in deformed single crystals, *Ultramicroscopy* 103 (2005) 33–39.
- [53] W. Pantleon, Resolving the geometrically necessary dislocation content by conventional electron backscattering diffraction, *Scr. Mater.* 58 (2008) 994–997.
- [54] B. El-Dasher, B. Adams, A. Rollett, Viewpoint: experimental recovery of geometrically necessary dislocation density in polycrystals, *Scr. Mater.* 48 (2003) 141–145.
- [55] C. Dahlberg, Y. Saito, M. Öztop, J. Kysar, Geometrically necessary dislocation density measurements associated with different angles of indentations, *Int. J. Plast.* 54 (2014) 81–95.
- [56] A. Godfrey, W.Q. Cao, Q. Liu, N. Hansen, Stored energy, microstructure, and flow stress of deformed metals, *Metall. Mater. Trans. A* 36 (2005) 2371–2378.
- [57] D.P. Field, C.C. Merriman, N. Allain-Bonasso, F. Wagner, Quantification of dislocation structure heterogeneity in deformed polycrystals by EBSD, *Modelling Simul. Mater. Sci. Eng.* 20 (2012) 024007.
- [58] J.K. Mason, J. Lind, S.F. Li, B.W. Reed, M. Kumar, Kinetics and anisotropy of the Monte Carlo model of grain growth, *Acta Mater.* 82 (2015) 155–166.
- [59] J.K. Mason, Grain boundary energy and curvature in Monte Carlo and cellular automata simulations of grain boundary motion, *Acta Mater.* 94 (2015) 162–171.
- [60] P.E. Goins, E.A. Holm, The Material Point Monte Carlo model: a discrete, off-lattice method for microstructural evolution simulations, *Comput. Mater. Sci.* 124 (2016) 411–419.
- [61] D. Raabe, Scaling Monte carlo kinetics of the Potts model using rate theory, *Acta Mater.* 48 (2000) 1617–1628.
- [62] M. Mueller, H. Knott, Beck, Deformation and recrystallization textures of rolled uranium sheet, *J. Met.* 203 (1955) 1214–1218.
- [63] C. Choi, M. Staker, Neutron diffraction texture study of deformed uranium plates, *J. Mater. Sci.* 31 (1996) 3397–3402.
- [64] J. Morrel, M. Jackson, *Uranium Processing and Properties*, Springer-Verlag, New York, 2013.
- [65] F. Bachmann, R. Hielscher, H. Schaeben, Texture analysis with MTEX - free and open source software toolbox, *Solid State Phenom.* 160 (2010) 63.
- [66] M. Steiner, J. Bhattacharyya, S. Agnew, The origin and enhancement of {0001} <11-20> texture during heat treatment of rolled AZ31B magnesium alloys, *Acta Mater.* 95 (2015) 443–455.
- [67] A. Beck, R. Sperry, Strain induced grain boundary migration in high purity aluminum, *J. Appl. Phys.* 21 (1950) 150.
- [68] G. Gottstein, L.S. Shvindlerman, *Grain Boundary Migration in Metals: Thermodynamics, Kinetics, Applications*, second ed., CRC Press, 2009.
- [69] E.S. Fisher, Preparation of alpha uranium single crystals by a grain-coarsening method, *J. Metals* 9 (1957) 882–888.
- [70] G. Marshall, J. Proust, Rogers, R. McCabe, Automatic twin statistics from electron backscattered diffraction data, *J. Microsc.* 238 (2010) 218–229.
- [71] S.D. Sintay, M.A. Grober, A.D. Rollet, 3D reconstruction of digital microstructures, in: *Electron Backscatter Diffraction in Materials Science*, second ed., Springer, 2009.
- [72] D. Mainprice, F. Bachman, R. Hielscher, H. Schaeben, Descriptive tools for the analysis of texture projects with large datasets using MTEX: strength, symmetry and components, *Special Publ. Geol. Soc. Lond.* 409 (2014) 251–271.
- [73] M. Knezevic, B. Drach, M. Ardeljan, I.J. Beyerlein, Three dimensional predictions of grain scale plasticity and grain boundaries using crystal plasticity finite element models, *Comput. Methods Appl. Mech. Eng.* 277 (2014) 239–259.
- [74] Z. Zeng, Y. Zhu, S. Xu, M. Bian, J. Nie, Texture evolution during static recrystallization of cold-rolled magnesium alloys, *Acta Mater.* 105 (2016) 479–494.